PAPER • OPEN ACCESS

Pre-set extrusion bioprinting for multiscale heterogeneous tissue structure fabrication

To cite this article: Donggu Kang *et al* 2018 *Biofabrication* **10** 035008

View the article online for updates and enhancements.

Related content

IOP ebooks™

Bringing you innovative digital publishing with leading voices to create your essential collection of books in STEM research.

Start exploring the collection - download the first chapter of every title for free.

Biofabrication

Pre-set extrusion bioprinting for multiscale heterogeneous tissue structure fabrication

Donggu Kang[1,5]**, Geunseon Ahn**[2,5]**, Donghwan Kim**[3]**, Hyun-Wook Kang**[4] iD**, Seokhwan Yun**[3]**, Won-Soo Yun**[2,3]**, Jin-Hyung Shim**[3,6]** and Songwan Jin**[3,6] iD

1   Department of Mechanical System Engineering, Korea Polytechnic University, Siheung, Republic of Korea
2   Research Institute, T&R Biofab Co. Ltd, 237, Siheung, Republic of Korea
3   Department of Mechanical Engineering, Korea Polytechnic University, Siheung, Republic of Korea
4   Biomedical Engineering, School of Life Sciences, Ulsan National Institute of Science and Technology, 50 UNIST-gil, Ulsan 44919, Republic of Korea
5   These authors equally contributed to this work.
6   Authors to whom any correspondence should be addressed.

E-mail: songwan@kpu.ac.kr and happyshim@kpu.ac.kr

Abstract

Recent advances in three-dimensional bioprinting technology have led to various attempts in fabricating human tissue-like structures. However, current bioprinting technologies have limitations for creating native tissue-like structures. To resolve these issues, we developed a new pre-set extrusion bioprinting technique that can create heterogeneous, multicellular, and multimaterial structures simultaneously. The key to this ability lies in the use of a precursor cartridge that can stably preserve a multimaterial with a pre-defined configuration that can be simply embedded in a syringe-based printer head. The multimaterial can be printed and miniaturized through a micro-nozzle without conspicuous deformation according to the pre-defined configuration of the precursor cartridge. Using this system, we fabricated heterogeneous tissue-like structures such as spinal cords, hepatic lobule, blood vessels, and capillaries. We further obtained a heterogeneous patterned model that embeds HepG2 cells with endothelial cells in a hepatic lobule-like structure. In comparison with homogeneous and heterogeneous cell printing, the heterogeneous patterned model showed a well-organized hepatic lobule structure and higher enzyme activity of CYP3A4. Therefore, this pre-set extrusion bioprinting method could be widely used in the fabrication of a variety of artificial and functional tissues or organs.

1. Introduction

Complex biological systems such as the human body are organized into hierarchical structures, with various cells arranged in tissues, organs, and finally the whole organism [1]. Thus, to fabricate mature three-dimensional (3D) tissues, biomanufacturing tools should be designed so as to be able to generate various multiscale structures. Toward this end, various multiscale assembly strategies have been developed based on self-assembly, guided assembly, and direct assembly strategies. However, most of these methods are still in the developmental stage with several challenges remaining in terms of assembly efficiency, speed, and mechanical stability [2]. In this context, 3D bioprinting technologies have recently emerged as attractive biomanufacturing tools with advantages of speed and convenience to effectively handle a wide diversity of cell types and biomaterials.

Dramatic advances in 3D bioprinting technologies have enabled the fabrication of artificial and functional tissues or organs owing to their versatility in terms of precise printing for the spatial positioning/patterning of each component on demand and the wide selectivity of biomaterials/biomolecules and cell types [3–5]. Therefore, these technologies have been applied in various biomedical engineering fields [6–8]. Extrusion-based bioprinting, a popular

and representative bioprinting technology, offers great flexibility for printing various materials (e.g., synthetic polymers and viscous bioinks) and allows for the creation of complex 3D structures. However, one of the drawbacks of this technology is that the cells extruded through the nozzle of the small diameter can be damaged by shear stress [9]. To overcome this limitation, a nozzle with a larger diameter has been used to reduce the shear stress. However, this diminishes its printing precision [10].

An additional challenge in fabricating complex and sophisticated 3D microstructures is that various materials need to be printed with elaborate patterns; hence, the current extrusion-based bioprinters employ multiple printing heads for the fabrication of complex biological structures [11–13]. However, an increased number of printing heads requires a more complex printing system and a long fabrication time. For these reasons, several research groups have applied microfluidics to bioprinting, which simultaneous dispenses multiple materials for the fabrication of more precise microstructures [7, 12–14]. Similarly, microfluidic-based spinning techniques with continuous coaxial flow have been developed to create fibrous tissue structures. These structures have a higher resolution than the current extrusion-based printing methods [15–18]. However, despite the many advantages of microfluidic bioprinting, it requires reservoirs with fluid controllers for each material and low-viscosity bioinks to reduce shear stress. Furthermore, because this technology is substantially based on continuous flow, the dispensed material needs to be solidified *in situ* at the end of the nozzle [7, 14, 16, 19–21].

Human tissues are extremely heterogeneous and comprised of different cells [22]. In particular, the hepatic lobule in the human liver tissue is a building block of the liver parenchyma, consisting of a portal triad, hepatocytes arranged in the liver cord within a sinusoid network, and a central vein. The cross-sectional diameter of a hepatic lobule is approximately 1 mm, while the diameter of the sinusoid is approximately several tens of micrometers, and the size of the whole liver is several tens of centimeters [23]. Therefore, a printing technique for the liver tissue should be able to reproduce structures at a wide size range from the micrometer to centimeter scale. Current precision bioprinting methods such as inkjet-based printing [24] and laser-assisted printing [25] have high-resolution; however, their applicability to the fabrication of large organs is limited. By contrast, while extrusion-based printing can help fabricate human-scale tissues [6], its resolution is not sufficiently high to reproduce microscale structures such as the sinusoid.

In this study, we developed a pre-set extrusion bioprinting method that allows for the *in situ* fabrication of heterogeneous artificial tissue-like structures. Various structures such as the spinal cord, hepatic lobule, capillary, blood vessels, and even an 'S'-shaped object

were fabricated heterogeneously to confirm the feasibility of pre-set extrusion bioprinting. Moreover, a tetramerous structure was fabricated by both pre-set extrusion and conventional bioprinting to compare cell viability with the two techniques. Further, endothelial cells (ECs) and HepG2 cells were heterogeneously co-printed by pre-set extrusion bioprinting, and the cell viability, proliferation, and enzyme activity of CYP3A4 in both groups (homogeneous or heterogeneous cell printing) were evaluated in parallel.

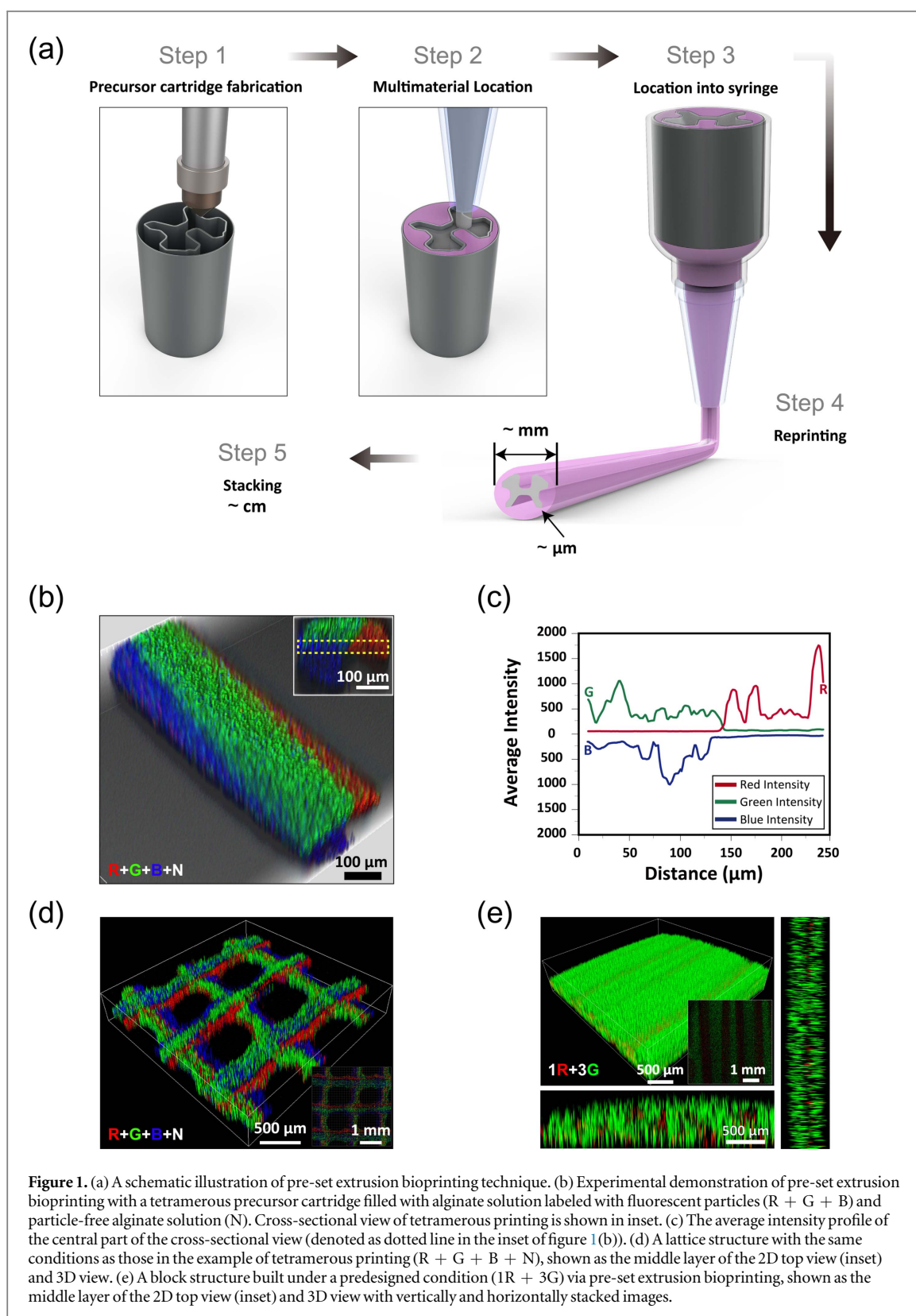## 2. Materials and methods

2.1. Materials
Sodium alginate (medium viscosity) and calcium chloride (anhydrous) were purchased from Sigma-Aldrich. Fluorescent particles (R0200B, G0200B, B0200; 2.0 μm, 2.0 μm, and 2.1 μm, respectively) and the LIVE/DEAD Viability/Cytotoxicity kit (L3224) were obtained from Fisher Scientific (UK). Lyophilized Atelo-collagen (Matrixen-PSP) derived from the porcine tendon was purchased from SKBioland (South Korea).

Various precursor cartridges with specific patterns of tetramerous shape, spinal cord, hepatic lobule, blood vessels, and the letter 'S' were designed using SolidWorks software (Dassault Systems, Vélizy-Villacoublay, France). The designs were then converted to STL-files and imported into commercial 3D printing system software for prototyping (ideaMaker, Shanghai Fusion Technology, China). Finally, various precursor cartridges were fabricated. The diameter of the tetramerous precursor cartridge was 9.3 mm, to fit into 3 ml syringes, and the other cartridges were 15 mm in diameter, to fit into a 10 ml syringe. The height of the tetramerous precursor cartridge was 15 mm and that of the other cartridges was 20 mm.

2.2. Bioink characterization and preparation
2.2.1. Alginate solutions
Solutions of 2.0%, 3.0%, and 4.0% (w/v) sodium alginate (viscosity $\geqslant$ 2000 cP, 25 °C) in distilled water were prepared and stirred for 24 h at 25 °C. Sequentially, the alginate solution was blended with red, green, and blue fluorescent particles, or without fluorescent particles. To visualize the myriad of tissue structures, the fluorescent particle-blended alginate solution was added to the empty segment of the cartridge, and then placed into the syringe. From this mixture, each fluorescent particle-blended alginate solution was simultaneously reprinted into a 200 mM CaCl$_2$ bath for solidification. The reprinted struts were then subjected to laser-scanning confocal microscopy (FV 1200, Olympus, Tokyo, Japan) by z-stacking (30 μm intervals) and reconstructed using laser-scanning confocal microscopy software. Using the same method as described in the preceding paragraph, the fluorescent particle-blended alginate solution was

Figure 1. (a) A schematic illustration of pre-set extrusion bioprinting technique. (b) Experimental demonstration of pre-set extrusion bioprinting with a tetramerous precursor cartridge filled with alginate solution labeled with fluorescent particles (R + G + B) and particle-free alginate solution (N). Cross-sectional view of tetramerous printing is shown in inset. (c) The average intensity profile of the central part of the cross-sectional view (denoted as dotted line in the inset of figure 1(b)). (d) A lattice structure with the same conditions as those in the example of tetramerous printing (R + G + B + N), shown as the middle layer of the 2D top view (inset) and 3D view. (e) A block structure built under a predesigned condition (1R + 3G) via pre-set extrusion bioprinting, shown as the middle layer of the 2D top view (inset) and 3D view with vertically and horizontally stacked images.

used for creating a lattice and block structure with layer-by-layer printing (figure 1(d)). The 2% and 4% alginate solutions were also used to demonstrate the applicability of our method with a wide range of viscous materials. The experimental details are shown in supplementary figure S1 is available online at stacks. iop.org/BF/10/035008/mmedia.

2.2.2. Collagen solutions

To create a neutral collagen solution (pH 7.4), a collagen solution (pH 4.0) was mixed with 10X Dulbecco's modified Eagle medium (DMEM) solution and reconstituted buffer (2.2 g $NaHCO_3$, 4.77 g HEPES, 0.2 g NaOH in 100 ml distilled water) at a volume ratio of 8:1:1. The neutralized collagen (5% w/v) was

mixed with HepG2 cells (HB-8065, American type culture collection (ATCC), USA) at a density of 3×10^7 cells ml^{-1} and EA.hy 926 cells (CRL-2922, ATCC, USA) at a density of 2×10^7 cells ml^{-1}. The final concentration of cell-laden collagen was 3%. For pre-gelation of collagen, the bioink (e.g., cell-laden collagen) was printed onto DMEM with 10% fetal bovine serum (FBS) and 5% penicillin/streptomycin at 37 °C for 1 h, and then cut by surgical blade and moved to a 24-well culture plate. The diameter of the bioprinted constructs was approximately 600 μm and the length was approximately 10 mm.

Rheological properties of the various alginate solutions and collagen with or without cells were measured using a Kinexus Pro + rheometer (Malvern, Worcestershire, UK) equipped with a geometric cone plate with a 20 mm diameter (PU20 SR3650 SS) and 1 mm gap. To prevent the gradual gelation of collagen, rheological analysis of collagen was performed at 4 °C, which was same as the printing temperature.

2.3. Fluorescent intensity analysis

The surface intensity profile from cross-sectional images of the myriad bioprinted constructs was analyzed using Matlab R2011a. In particular, to visualize two-dimensional surface images, red, green, and blue fluorescent intensities were normalized equally.

2.4. Miniaturization of tetramerous printing

To assess the degree of miniaturization (the percentage ratio of a single strut to a quarter of a strut) in a single strut of tetramerous printing, various nozzle sizes were tested. The cross-sectional view was obtained from z-stacked images (intervals of 30 μm) using laser-scanning confocal microscopy. The whole area of the strut, including the red, green, and blue fluorescent particles and the particle-free alginate solution, was defined as a single strut, and the area of one of the red, green, or blue fluorescent particles was defined as a quarter of a strut.

For precise comparison of the diameter between a single strut and a quarter of a strut, the hydraulic diameter, i.e., the equivalent diameter for an uneven-shaped strut, was applied. The hydraulic diameters of the single and quarter of a strut could then be directly compared. An example of this methodology and its application are shown in supplementary figure S2.

2.5. Cell culture

The NIH/3T3 (CRL-1658, ATCC, USA), HepG2, and EA.hy 926 cell lines were obtained from the ATCC and cultured in DMEM (Gibco, UK) supplemented with 10% FBS (Gibco, UK) and 1% penicillin/streptomycin (Gibco, UK) at 37 °C under 5% CO_2. When the cells reached confluence, they were detached from the culture dish using 0.25% trypsin (Thermo Fisher, USA) and then blended with the prepared alginate solutions at room temperature or prepared collagen on ice before bioprinting.

2.6. Cell viability

To assess cell viability, the cell-laden alginate solution was placed into printer head. After printing, the live/dead assay was conducted to determine the cell viability using calcein AM and ethidium homodimer-1. The live and dead cells were captured by laser-scanning confocal microscopy with z-stacking (30 μm intervals). At least 10 randomly selected areas of each sample were used to analyze cell viability (figures 3(d), (e)).

In the experimental group of haptic lobule printing, the cell-laden collagen was cut by a surgical blade (approximately 1 mm) to visualize cross-section of printed strut. The live/dead assay was then performed as described above (figure 5(c)).

2.7. Cell proliferation

Cell proliferation was measured using Cell Counting Kit-8 (CCK-8; Dojindo Molecular Technologies, USA), as described previously [26]. In brief, the bioprinted strut was exposed to fresh culture medium and CCK-8 reagent at a ratio of 10:1 after incubation for 1, 3, and 5 d. The absorbance was then measured at a wavelength of 450 nm using a multimode microplate reader (Bioteck, USA).

2.8. Enzyme activity of CYP3A4

The CYP3A4 activity was evaluated using the P450-GloTM CYP3A4 assay kit (Promega, USA) according to the manufacturer's instructions. The bioprinted constructs were treated with rifampicin (25 μM) for 6 h for induction and were then medium-aspirated. The bioprinted construct was incubated with culture medium supplemented with 50 μM CYP3A4 substrates. At 1 h after treatment, 50 μl of the culture medium was removed and activity of the sample was assayed in a luminometer.

2.9. Immunofluorescence staining

Immunofluorescence staining was applied to visualize cell morphology using 4′,6-diamidino-2-phenylindole (DAPI; D1306, Invitrogen, USA), phalloidin Alexa Fluor 594 (A34055, Invitrogen, USA), phalloidin Aelxa Fluor 488 (A12379, Invitrogen, USA) and cluster of differentiation 31 (CD31) primary antibody (ab9498, Abcam, UK).

After culture for 1, 3, and 5 d, we used immunofluorescence staining (DAPI, phalloidin) to observe the surface of printed collagen constructs (figure 5(d)): each construct was fixed in ice cold 4% paraformaldehyde (WAKO, Japan) and rinsed with PBS. The fixed constructs were permeabilized with 0.2% Triton-X 100 for 10 min, and then sequentially stained with phalloidin (green) and DAPI (blue).

Likewise, to observe the cross-section of printed collagen constructs (figure 5(e)), the sample was cut by surgical blade (approximately 1 mm). The fixed and permeabilized constructs were then blocked with 1% bovine serum albumin (BSA, GenDEPOT) and immunostained using a primary antibody against CD31 (1:200) for 1 h. The samples were incubated with Alexa Fluor 488 goat anti-mouse (1:500) for CD31 for 1 h. All samples were counterstained with DAPI (blue) and phalloidin (red) and visualized using a laser-scanning confocal microscope.

To visualize the overall structure of the bioprinted strut, the EA.hy 926 cells were stained with Cell Tracker Red CMTPX Dye (C34552, Invitrogen, USA) and HepG2 cells were stained with Cell Tracker Green CMFDA Dye (C2925, Invitrogen, USA). Both cell types were blended with collagen, and then placed in the printer head. After printing, the constructs were captured by laser-scanning confocal microscopy with z-stacking (30 μm intervals) (figure 5(b)).

2.10. Statistical analysis
Three independent replicates were performed for all experiments. The statistical software SPSS 18.0 (SPSS Inc., Chicago, IL, USA) was used for data analysis. Data are expressed as the mean $\pm$ standard deviation. Significant differences were assessed by a non-parametric Mann–Whitney U test. A value of $p < 0.05$ was judged as a statistically significant difference.

3. Results and discussion

3.1. Pre-set extrusion bioprinting
As shown in figure 1, we first designed and fabricated the precursor cartridge, which is compartmentalized into several segments, using a commercial 3D printing apparatus (figure 1; Step 1). The cross-sectional shape of the precursor cartridge can be manipulated freely to allow for versatile shapes and structures. Second, each cartridge was filled with different types of bioinks as desired (Step 2) and placed into a syringe (Step 3). The multiple materials (i.e., multiple bioinks) were extruded through the printing nozzle and three-dimensionally materialized, with the same cross-sectional shape as that of the precursor cartridge (Step 4). In addition, the single multimaterial struts could be stacked to create the intended large-scale tissue structures (Step 5). Thus, the key element of our new strategy is the adoption of a precursor cartridge, which is designed to fit into a printer head with compartmentalization for the multiple bioinks. When the bioinks are extruded through a small nozzle, the cross-sectional shape is miniaturized three-dimensionally, and is able to well-retain the initial shape. This technique is based on the well-established concept that fluids with a small Reynolds number do not mix easily and maintain their original flow patterns [12, 27].
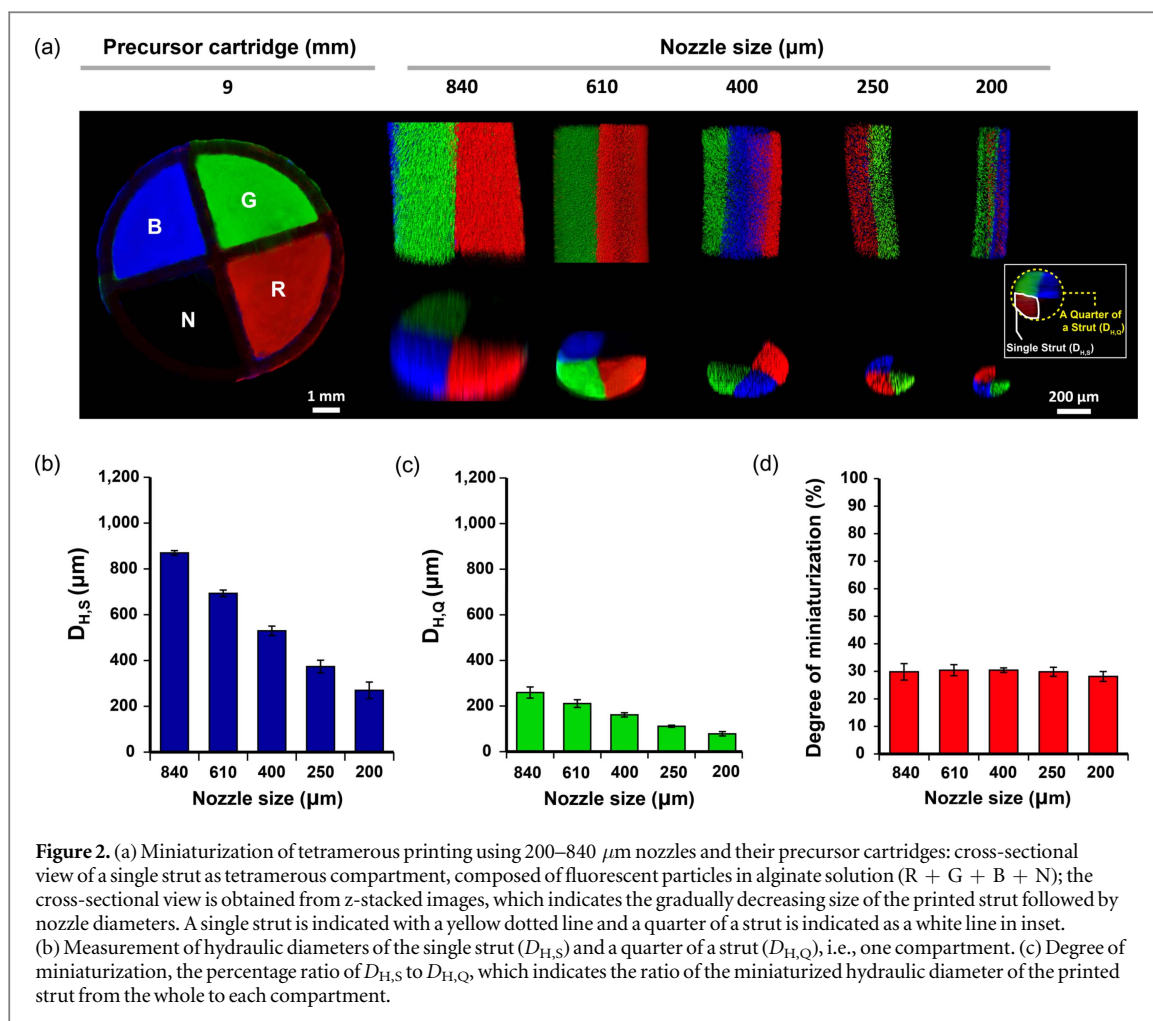
As a proof-of-concept of the applicability of this technique, we first employed a tetramerous cartridge consisting of a 3% w/v alginate solution, containing three different fluorescent particles (red (R), green (G), and blue (B)) and a particle-free alginate solution (N), respectively, filled into each segment. The alginate solution was then dispensed into 200 mM calcium chloride ($CaCl_2$) through the nozzle. The single strut (R + G + B + N) could be dispensed while maintaining the tetramerous shape (figures 1(b), (c)). Similar results were obtained with various viscosities of the bioink (supplementary figure S1). We also successfully created a 3D construct of a simple square lattice (R + G + B + N) and a multilayer block structure (1R + 3G) (figure (d), (e)).

3.2. Miniaturization of tetramerous printing
We next compared the diameters of a single strut (R + G + B + N) and a quarter of a strut (R or G or B), which were extruded through the nozzles with various inner diameters (840 μm, 610 μm, 400 μm, 250 μm, and 200 μm; figure 2(a)). In addition, the hydraulic diameter (D_H = 4 × cross-sectional area of strut/perimeter of strut) was applied for more precise comparisons (supplementary figure S2). The hydraulic diameter of the single strut ($D_{H,S}$) was similar to the nozzle size (figure 2(b)), and those of a quarter of a strut ($D_{H,Q}$) were approximately 260 μm, 211 μm, 161 μm, 111 μm, and 76 μm, respectively, (figure 2(c)). Although the size of each printed strut (i.e., $D_{H,S}$) was significantly different according to the nozzle size, the degrees of miniaturization ($D_{H,Q}/D_{H,S}$ × 100) were fairly consistent ($\approx$30%) (figure 2(d)). This result demonstrates that the pre-set extrusion bioprinting method enhanced the printing resolution by more than 3.3 times in this case (i.e., using a tetramerous precursor cartridge) compared to the same printing conditions but without a precursor cartridge. Therefore, the multiple bioinks in the precursor cartridge could be miniaturized consistently with a well-retained cross-sectional shape of the precursor cartridge.

3.3. Comparison between conventional bioprinting and pre-set extrusion bioprinting
We next aimed to assess the effect of nozzle size on cell viability using nozzles of different sizes (inner diameter (I.D.): 610, 400, 250, or 200 μm) and over time (at 0, 15, 30, 45, 60, or 120 min after printing). The NIH/3T3-laden bioinks were dispensed without the precursor cartridge, and a live/dead assay was performed under set conditions (i.e., different nozzle sizes and printing times). Cell viability was significantly lower on nozzles of relatively smaller sizes (250 and 200 μm) with a culture duration of 120 min than that on nozzles with larger sizes (400 and 610 μm) (figure 3(b)). In addition, the dead cells (red) were mostly detected at the peripheral

Figure 2. (a) Miniaturization of tetramerous printing using 200–840 μm nozzles and their precursor cartridges: cross-sectional view of a single strut as tetramerous compartment, composed of fluorescent particles in alginate solution (R + G + B + N); the cross-sectional view is obtained from z-stacked images, which indicates the gradually decreasing size of the printed strut followed by nozzle diameters. A single strut is indicated with a yellow dotted line and a quarter of a strut is indicated as a white line in inset. (b) Measurement of hydraulic diameters of the single strut ($D_{H,S}$) and a quarter of a strut ($D_{H,Q}$), i.e., one compartment. (c) Degree of miniaturization, the percentage ratio of $D_{H,S}$ to $D_{H,Q}$, which indicates the ratio of the miniaturized hydraulic diameter of the printed strut from the whole to each compartment.

area of the printed strut at 0 min (figure 3(a)), indicating the potential for damage by wall shear stress. As a result, the cell viability gradually decreased with a decrease in nozzle size and an increase in time.

Creating the same tetramerous structure (figure 1(b)) using the conventional bioprinting technique would require four heads (one for each material) (figure 3(c)). Therefore, it necessarily took more time and needed a complicated printing system. As shown in figure 3(d), we successfully fabricated a tetramerous structure using pre-set extrusion bioprinting (nozzle I.D. = 610 μm) and conventional bioprinting (nozzle I.D. = 250 μm). The conventional printing technique resulted in lower cell viability than the pre-set extrusion bioprinting technique, which was attributed to the difference in nozzle size (figure 3(e)). Thus, the proposed strategy of pre-set extrusion bioprinting has advantages that enable *in situ* heterogeneous multimaterial bioprinting in a simple manner, which improves cell survival.

3.4. Applicability of pre-set extrusion bioprinting
Precise cell patterning techniques to mimic the complicated microstructures of native tissues are important and challenging, because only the accurate

positioning of different cell types and choice of biomaterials can provide the adequate niche for tissue formation [4]. We tested the applicability of our technique for a variety of complex heterogeneous structures such as the spinal cord, hepatic lobule, capillaries, blood vessels, and even an 'S'-shaped object (figures 4(a)–(e)). As shown in the first column in figure 4, we designed the geometric shape of the precursor cartridges using 3D CAD modeling based on the various human tissues, and the letter 'S'. The precursor cartridge was fabricated by rapid prototyping (figure 4, second column), and then multiple materials (e.g., bioinks) were added to fill each segment. The printed constructs were then extruded according to the pre-defined configurations: design of precursor cartridge and material segmentation (figure 4, third column). The surface intensity plot of the cross-section shown in the fourth column of figure 4 indicates that a diversified form with multiple materials can be printed.

Among the biological structures, the spinal cord is an irregular cylinder separated by white and gray matter, and the hepatic lobule is a heterogeneous structure of a dense portion containing a large number of hepatocytes and sinusoids. In terms of printing resolution, a 3D structure that accurately mimics these tissues was
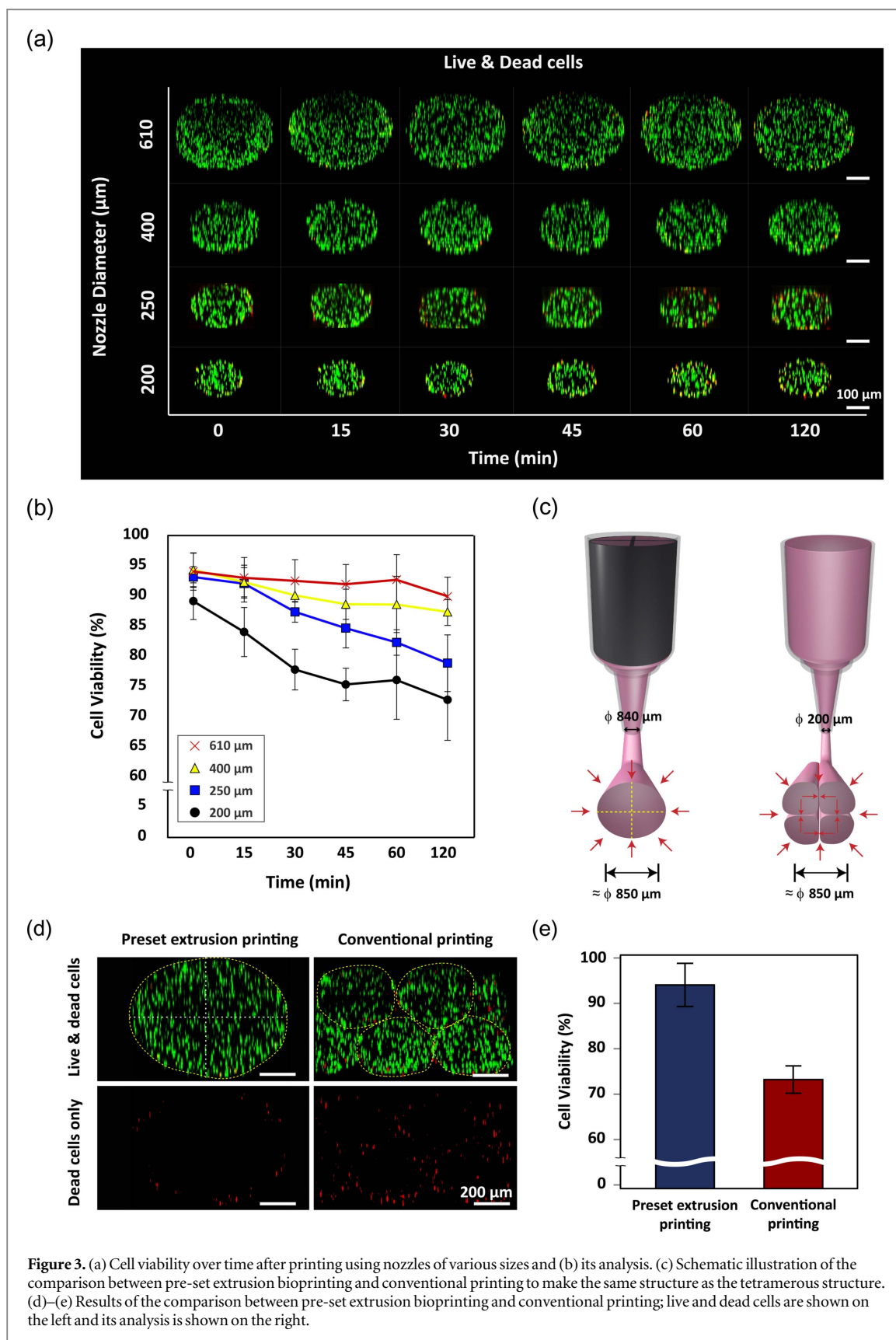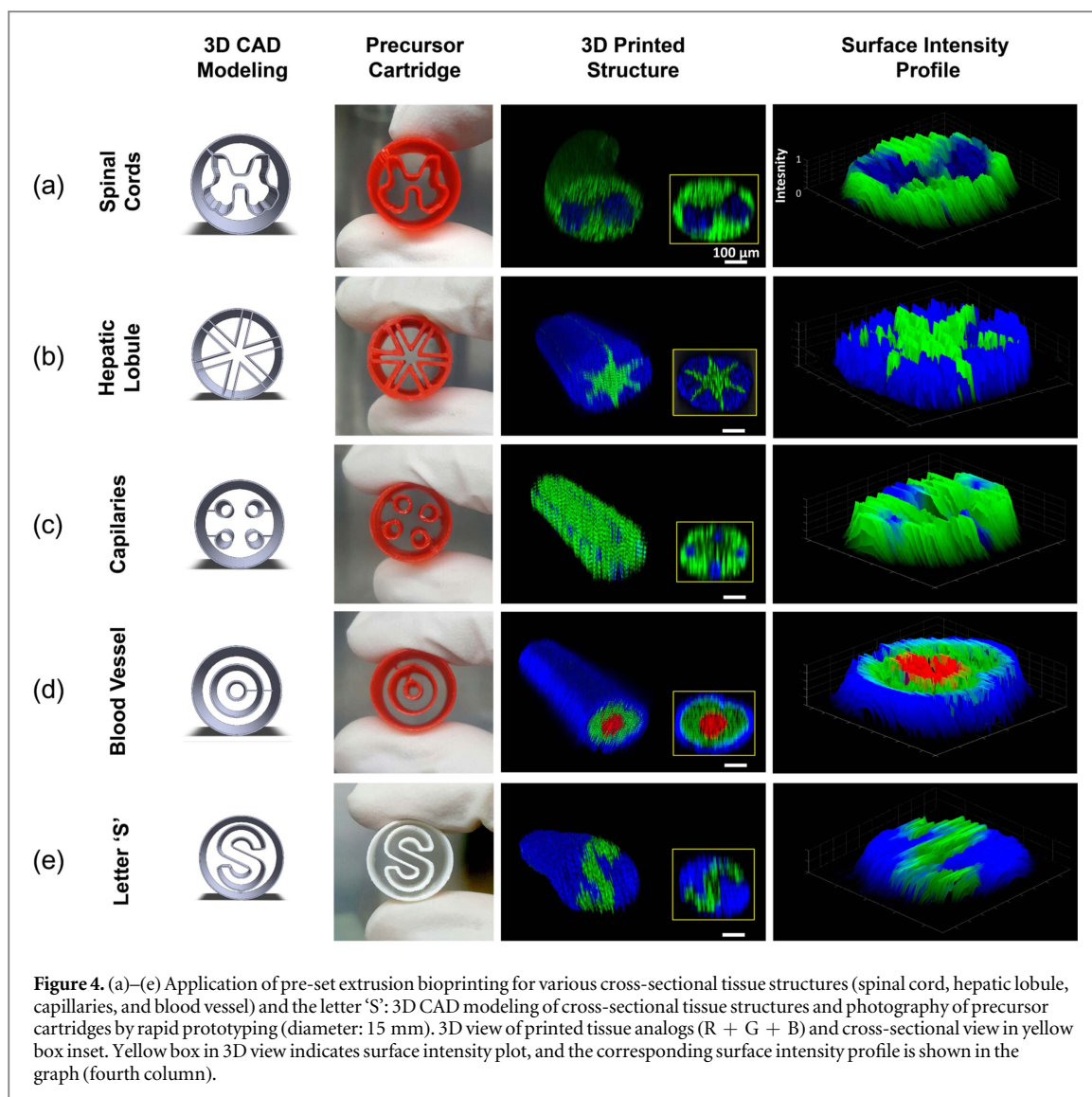
Figure 3. (a) Cell viability over time after printing using nozzles of various sizes and (b) its analysis. (c) Schematic illustration of the comparison between pre-set extrusion bioprinting and conventional printing to make the same structure as the tetramerous structure. (d)–(e) Results of the comparison between pre-set extrusion bioprinting and conventional printing; live and dead cells are shown on the left and its analysis is shown on the right.

difficult to create using the conventional bioprinting method. This is because a patterning technique must be precise (100 μm or less) [28] while maintaining high cell viability [29]. In demonstrating our proof-of-concept, we have shown the ability of our method to successfully produce heterogeneous 3D structures. The significance of this method is that the precursor cartridges can formulate various sophisticated heterogeneous structures as desired, with a simple system configuration.
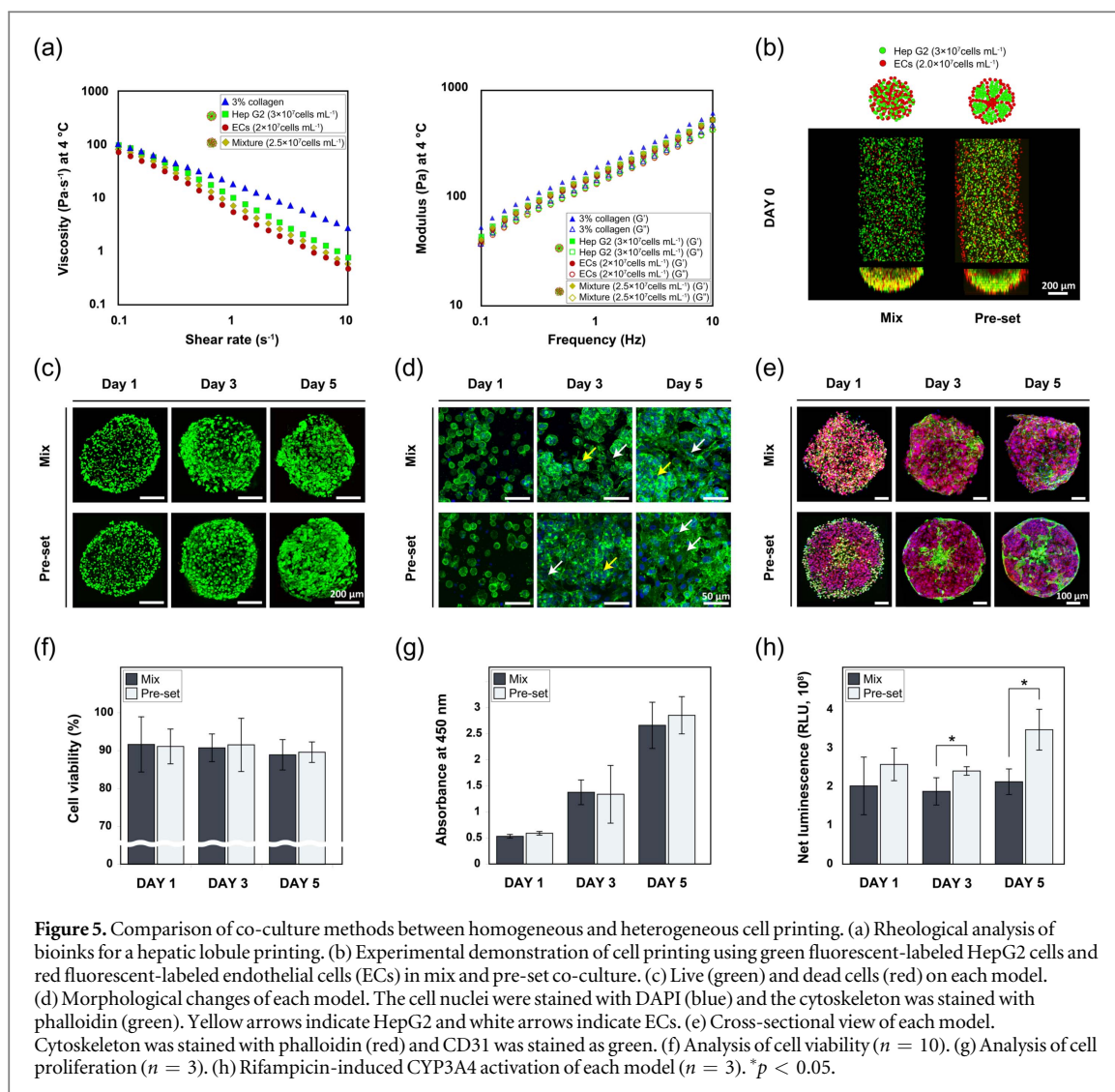
Figure 4. (a)–(e) Application of pre-set extrusion bioprinting for various cross-sectional tissue structures (spinal cord, hepatic lobule, capillaries, and blood vessel) and the letter 'S': 3D CAD modeling of cross-sectional tissue structures and photography of precursor cartridges by rapid prototyping (diameter: 15 mm). 3D view of printed tissue analogs (R + G + B) and cross-sectional view in yellow box inset. Yellow box in 3D view indicates surface intensity plot, and the corresponding surface intensity profile is shown in the graph (fourth column).

3.5. Hepatic lobule printing

Most biological systems are characterized by a multilevel hierarchical structure, spanning a broad scale ranging from the macroscopic to microscopic level [2]. The liver is also a representative complex organ with several interconnected structures across several scales. In addition, the liver is responsible for drug and toxin metabolism, which is crucial to survival. Thus, generation of an appropriate liver model is a promising method for studying drug metabolism and toxicological responses [30]. Herein, we fabricated two different co-culture models consisting of ECs and HepG2 cells by pre-set extrusion bioprinting (Pre-set) or a simple cell mixing printing (Mix). A modified design for hepatic lobule printing was also newly developed, as shown in the Supplementary Information (supplementary figure S3).

The results of the rheological analysis of the four different bioinks (HepG2-laden collagen, ECs-laden collagen, mixture-laden collagen, and collagen only) are shown in figure 5(a). The viscosity, storage modulus (G'), and loss modulus (G'') of collagen were

slightly higher than those of cell-laden collagen (figure 5(a)). Nevertheless, the hepatic lobule structure was successfully fabricated (figure 5(b)). After 5 d of culture, the viability of the cells on each construct was still close to 90% (figures 5(c), (f)). In addition, the proliferation of both cell types on the printed constructs was not significantly changed between day 1 and day 3 (figure 5(g)). Thus, a cellular niche, i.e., the printed constructs, was cytophilic for both cell types. Sequentially, we found that the heterogeneous patterning could facilitate the connectivity of each cell type. As shown in figure 5(d), ECs on the Pre-set covered the surface of the collagen with cell–cell junctions. However, the homogeneously mixed cells were delayed or irregular in forming cell–cell connections. Cross-sectional view of the printed construct showed similar results (figure 5(e)). Furthermore, despite the similar levels of cell viability and proliferation on both the Mix and Pre-set, rifampicin-induced CYP3A4 activation on HepG2 cells was significantly higher in the Pre-set than in the Mix (figure 5(h)). Therefore, homogeneous and heterogeneous patterned co-culture

Figure 5. Comparison of co-culture methods between homogeneous and heterogeneous cell printing. (a) Rheological analysis of bioinks for a hepatic lobule printing. (b) Experimental demonstration of cell printing using green fluorescent-labeled HepG2 cells and red fluorescent-labeled endothelial cells (ECs) in mix and pre-set co-culture. (c) Live (green) and dead cells (red) on each model. (d) Morphological changes of each model. The cell nuclei were stained with DAPI (blue) and the cytoskeleton was stained with phalloidin (green). Yellow arrows indicate HepG2 and white arrows indicate ECs. (e) Cross-sectional view of each model. Cytoskeleton was stained with phalloidin (red) and CD31 was stained as green. (f) Analysis of cell viability ($n = 10$). (g) Analysis of cell proliferation ($n = 3$). (h) Rifampicin-induced CYP3A4 activation of each model ($n = 3$). $^*p < 0.05$.

did not affect cell proliferation but did influence individual cell–cell interactions, indicating that the cellular function can also be directly influenced by heterogeneous cell printing.

Taken together, these results confirmed the utility of pre-set extrusion bioprinting using both alginate and collagen bioinks that are widely applied materials for bioprinting. Further, a hepatic lobule construct was successfully fabricated using pre-set extrusion bioprinting. Overall, this study demonstrates that heterogeneous cell printing could improve cellular functionality compared to homogeneous cell printing.

4. Conclusions

In this study, we developed a pre-set extrusion bioprinting technique for creating artificial tissues or organs. The concept involves the use of a precursor cartridge, from which various cross-sectional tissue structures such as the hepatic lobule, spinal cord, capillaries, blood vessels, and even a letter-shaped object can be printed. Therefore, benefiting from high-resolution multimaterial printing of diverse structures with a simple system configuration, the proposed pre-set extrusion bioprinting technique could be used in a wide range of 3D printing applications overcoming the key limitations of conventional biofabrication technologies.

ORCID iDs

Hyun-Wook Kang ⓘ https://orcid.org/0000-0001-5335-5604
Songwan Jin ⓘ https://orcid.org/0000-0002-1540-7765

References

[1] Lobo I 2008 Biological complexity and integrative levels of organization *Nat. Educ.* **1** 141

[2] Guven S, Chen P, Inci F, Tasoglu S, Erkmen B and Demirci U 2015 Multiscale assembly for tissue engineering and regenerative medicine *Trends Biotechnol.* **33** 269–79

[3] Kolesky D B, Truby R L, Gladman A, Busbee T A, Homan K A and Lewis J A 2014 3D bioprinting of vascularized, heterogeneous cell-laden tissue constructs *Adv. Mater.* **26** 3124–30

[4] Pati F, Jang J, Ha D-H, Kim S W, Rhie J-W, Shim J-H, Kim D-H and Cho D-W 2014 Printing three-dimensional tissue analogues with decellularized extracellular matrix bioink *Nat. Commun.* **5** 3935

[5] Kolesky D B, Homan K A, Skylar-Scott M A and Lewis J A 2016 Three-dimensional bioprinting of thick vascularized tissues *Proc. Natl Acad. Sci.* **113** 3179–84

[6] Kang H-W, Lee S J, Ko I K, Kengla C, Yoo J J and Atala A 2016 A 3D bioprinting system to produce human-scale tissue constructs with structural integrity *Nat. Biotechnol.* **34** 312–9

[7] Liu W, Zhang Y S, Heinrich M A, De Ferrari F, Jang H L, Bakht S M, Alvarez M M, Yang J, Li Y C and Trujillo-de Santiago G 2017 Rapid continuous multimaterial extrusion bioprinting *Adv. Mater.* **29** 3

[8] Hinton T J, Jallerat Q, Palchesko R N, Park J H, Grodzicki M S, Shue H-J, Ramadan M H, Hudson A R and Feinberg A W 2015 Three-dimensional printing of complex biological structures by freeform reversible embedding of suspended hydrogels *Sci. Adv.* **1** e1500758

[9] Nair K, Gandhi M, Khalil S, Yan K C, Marcolongo M, Barbee K and Sun W 2009 Characterization of cell viability during bioprinting processes *Biotechnol. J.* **4** 1168–77

[10] Blaeser A, Duarte Campos D F, Puster U, Richtering W, Stevens M M and Fischer H 2016 Controlling shear stress in 3D bioprinting is a key factor to balance printing resolution and stem cell integrity *Adv. Healthcare Mater.* **5** 326–33

[11] Shim J-H, Lee J-S, Kim J Y and Cho D-W 2012 Bioprinting of a mechanically enhanced three-dimensional dual cell-laden construct for osteochondral tissue engineering using a multi-head tissue/organ building system *J. Micromech. Microeng.* **22** 085014

[12] Ober T J, Foresti D and Lewis J A 2015 Active mixing of complex fluids at the microscale *Proc. Natl Acad. Sci.* **112** 12293–8

[13] Hardin J O, Ober T J, Valentine A D and Lewis J A 2015 Microfluidic printheads for multimaterial 3D printing of viscoelastic inks *Adv. Mater.* **27** 3279–84

[14] Colosi C, Shin S R, Manoharan V, Massa S, Costantini M, Barbetta A, Dokmeci M R, Dentini M and Khademhosseini A 2016 Microfluidic bioprinting of heterogeneous 3D tissue constructs using low-viscosity bioink *Adv. Mater.* **28** 677–84

[15] Yu Y, Fu F, Shang L, Cheng Y, Gu Z and Zhao Y 2017 Bioinspired helical microfibers from microfluidics *Adv. Mater.* **29** 18

[16] Cheng Y, Zheng F, Lu J, Shang L, Xie Z, Zhao Y, Chen Y and Gu Z 2014 Bioinspired multicompartmental microfibers from microfluidics *Adv. Mater.* **26** 5184–90

[17] Shang L, Fu F, Cheng Y, Yu Y, Wang J, Gu Z and Zhao Y 2017 Bioinspired multifunctional spindle-knotted microfibers from microfluidics *Small* **13** 4

[18] Ouyang L, Yao R, Zhao Y and Sun W 2016 Effect of bioink properties on printability and cell viability for 3D bioplotting of embryonic stem cells *Biofabrication* **8** 035020

[19] Yu Y, Wei W, Wang Y, Xu C, Guo Y and Qin J 2016 Simple spinning of heterogeneous hollow microfibers on chip *Adv. Mater.* **28** 6649–55

[20] Grolman J M, Zhang D, Smith A M, Moore J S and Kilian K A 2015 Rapid 3D extrusion of synthetic tumor microenvironments *Adv. Mater.* **27** 5512–7

[21] Akbari M, Tamayol A, Laforte V, Annabi N, Najafabadi A H, Khademhosseini A and Juncker D 2014 Composite living fibers for creating tissue constructs using textile techniques *Adv. Funct. Mater.* **24** 4060–7

[22] Mescher A 2011 *Basic Histology* ed M Naderan and S M H Noori Moogehi 1st edn (Tehran: Teimourzadeh Publications)

[23] Crawford A R, Lin X Z and Crawford J M 1998 The normal adult human liver biopsy: a quantitative reference standard *Hepatology* **28** 323–31

[24] Singh M, Haverinen H M, Dhagat P and Jabbour G E 2010 Inkjet printing—process and its applications *Adv. Mater.* **22** 673–85

[25] Nahmias Y, Schwartz R E, Verfaillie C M and Odde D J 2005 Laser-guided direct writing for three-dimensional tissue engineering *Biotechnol. Bioeng.* **92** 129–36

[26] Kang D, Kim J H, Jeong Y H, Kwak J-Y, Yoon S and Jin S 2016 Endothelial monolayers on collagen-coated nanofibrous membranes: cell–cell and cell–ECM interactions *Biofabrication* **8** 025008

[27] Groisman A and Steinberg V 2001 Efficient mixing at low Reynolds numbers using polymer additives *Nature* **410** 905–8

[28] Duan B, Hockaday L A, Kang K H and Butcher J T 2013 3D bioprinting of heterogeneous aortic valve conduits with alginate/gelatin hydrogels *J. Biomed. Mater. Res.* A **101** 1255–64

[29] Ma X, Qu X, Zhu W, Li Y-S, Yuan S, Zhang H, Liu J, Wang P, Lai C S E and Zanella F 2016 Deterministically patterned biomimetic human iPSC-derived hepatic model via rapid 3D bioprinting *Proc. Natl Acad. Sci.* **113** 2206–11

[30] Diaz Ochoa J G, Bucher J, Péry A R, Zaldivar Comenges J M, Niklas J and Mauch K 2013 A multi-scale modeling framework for individualized, spatiotemporal prediction of drug effects and toxicological risk *Front. Pharmacol.* **3** 204